Radar Signature Prediction Using Moment Method Codes via a Frequency Extrapolation Technique

Yuanxun Wang, *Student Member, IEEE,* and Hao Ling, *Fellow, IEEE*

***Abstract*— A frequency extrapolation scheme is developed to efficiently predict radar signatures using moment method codes. The approach is to parameterize the induced current on the target based on a multipath excitation model via the ESPRIT superresolution algorithm. The multiple scattering mechanisms at high frequencies are included in the model to ensure the accuracy of the algorithm. The range profiles for several test targets are calculated to demonstrate the performance of the algorithm. A numerical experiment is conducted to find the possible error sources of the algorithm and determine an upper limit on the frequency extrapolation bandwidth. The algorithm is also extended to generate ISAR images by using the frequency extrapolation in conjunction with the bistatic approximation in the angular dimension. The ISAR image of the benchmark VFY-218 airplane is predicted at 400 MHz and compared against the chamber measurement result. The main scattering features in the measured image are successfully predicted using this approach with very modest computational resources.**

***Index Terms*—Frequency extrapolation, moment method.**

I. Introduction

PREDICTING the radar signatures of real targets by computer simulation is a problem of current interest. The traditional method of moments (MoM) is capable of handling complex geometrical models and can give very accurate results. However, it scales poorly in frequency and requires huge computation time and memory for targets with large electrical dimensions. Recently, with the emergence of the fast multipole method (FMM) and the multilevel fast multipole method (MLFMM) [1], [2], the computation complexity of the MoM has been significantly reduced. Radar cross section (RCS) computation can now be carried out for complex three-dimensional (3-D) targets above the resonant region and into the high-frequency regime on a desktop workstation. In practical applications, however, the simulation of radar signatures such as one-dimensional (1-D) range profiles and two-dimensional (2-D) inverse synthetic aperture radar (ISAR) imagery requires that the RCS be computed over many frequencies and aspects. In this paper, we present a frequency extrapolation technique to efficient construct the range profiles and ISAR images using the MoM.

Manuscript received March 15, 1998; revised November 20, 1998. This work was supported by the Air Force MURI Center for Computational Electromagnetics under Contract AFOSR F49620-96-1-0025.

The authors are with the Department of Electrical and Computer Engineering, The University of Texas at Austin, Austin, Texas 78712 USA.

Publisher Item Identifier S 0018-926X(99)05808-1.

Our approach to the frequency extrapolation problem is based on model-based parameter estimation [3]–[7]. We first parameterize the current at each point on the target surface based on a multipath exponential model. The model parameters include the times-of-arrival and excitation amplitudes. They are extracted via the estimation of signal parameters via rotational invariance techniques (ESPRIT) superresolution algorithm [8], [9] from a limited number of frequency samples of target current computed using the MoM. Once the model parameters are determined, the frequency response of the current is extrapolated. The scattered far field of the target over a broad frequency band can thus be computed from which the radar signature can be formed. It is well known that the key to the success of any extrapolation algorithm is an appropriate model for the observable of interest that coincides with the underlying physical mechanisms. Our proposed technique utilizes two important assumptions based on our existing knowledge of the problem physics. First, we use an exponential model instead of the often-used rational function model. As we shall show, this model is consistent with high-frequency ray-optical phenomenon and is the key to achieving large extrapolation bandwidth based on data computed at the low end of the high-frequency region. Second, we choose to parameterize the induced current on the target instead of the scattered field. This is because at frequencies above target resonance, only a small number of interactions are needed to adequately model the induced current at each point on the target. The scattered field, on the other hand, requires far more terms to model adequately for a complex target [10]. This implies that a larger number of frequency points are needed from the MoM calculation to properly estimate the model parameters for the scattered field.

Some preliminary results of our study have been reported earlier in a short letter [6]. In this paper, a more in-depth discussion on the algorithm is presented. In Section II, we first describe the multipath excitation model for the induced current and the superresolution algorithm to estimate the parameters in the model. This approach is applied to range profile extrapolation for 2-D and 3-D scatterers to show the effectiveness of the algorithm in Section III. In Section IV, we investigate the limitations and assess the general performance of the algorithm by conducting numerical tests on a canonical dihedral scatterer. In Section V, we extend the algorithm for ISAR image prediction by using the frequency extrapolation scheme in conjunction with the bistatic approximation in the angular dimension. The predicted image is compared against

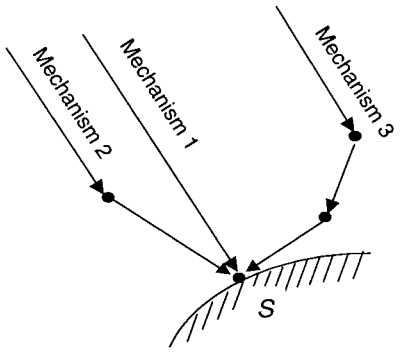

Fig. 1. Multipath excitation model of the scattering mechanisms.

the measured results on the benchmark VFY-218 airplane at 400 MHz [11]. Some conclusions are given in Section VI.

II. Exponential Current Model and Parameter Estimation

To construct a frequency-dependent model for the target current, we postulate that in the high-frequency region, the induced current at each point S on the target is excited by the incident as well as multiply scattered waves from other parts of the target, as illustrated in Fig. 1. Since each scattered wave component travels a different path to S, the current at S can be written as

$$J(f,S)=\sum_{i=1}^{N}A_i(S)\exp[-j2\pi f t_i(S)] \tag{1}$$

where f is the frequency and (A_i,t_i) are, respectively, the amplitude and time-of-arrival of the ith scattering mechanism. Three comments are in order. First, this model takes into account of the multiple scattering phenomenon. If point S lies in the lit region of the incident wave, the first term of the expansion would correspond to the physical optics current. The other terms have longer times-of-arrival and represent multiple scattering contributions from other parts of the target. At frequencies above target resonance, it is expected only a few terms in the expansion will be necessary to accurately model the actual current. Second, in our model A_i is assumed to be independent of frequency. As will be shown in Section IV, it is also possible to incorporate a frequency dependence into the amplitude parameter to achieve better extrapolation performance, provided enough frequency sampling points are available. Third, for 3-D MoM algorithms that use edge-based basis functions, the target surface is usually divided into a finite number of triangular facets. The induced current is then written as a sum of basis functions weighted by the current at the edges of the facet. Hence, extrapolation of the induced current on the target surface is equivalent to extrapolation of the current values at the edges of each facet.

Next, we apply the superresolution algorithm ESPRIT [8], [9] at all the current bases on the target to extract the model parameters (A_i,t_i) from a limited number of frequency samples of the target current calculated using the MoM. ESPRIT is a parameter estimation algorithm that can perform effectively in the presence of white Gaussian noise. It is based on the data model

$$F(f_m)=\sum_{i=1}^{N}A_i e^{-j2\pi f_m t_i}+n(f_m),\quad f_m=f_1,f_2,\cdots,f_M \tag{2}$$

where $n(\cdot)$ denotes additive white Gaussian noise and the samples are uniformly spaced. In comparison to earlier spectral estimation methods such as Prony's method, ESPRIT exploits the above underlying data model, which assumes cisoids in additive noise rather than pure cisoids. This yields estimates that are asymptotically unbiased and more robust than Prony's method when noise exists. If the data sequence obeys the underlying model exactly and the number of the sampling points M is infinite, ESPRIT can estimate N and resolve each A_i and t_i without any error. For finite-length data, the minimum number of samples to perform the estimation is $M>2N+1$ and the accuracy of the estimated parameters will depend on the length of the available data and how well the actual data fit the model.

The extrapolation procedure is as follows. First, we run the MoM code at M frequencies and save the current output at those frequencies. We then apply ESPRIT to the current values at M frequencies. The frequency-dependent current model in (1) can thus be obtained. Once such a model is found, the data are extrapolated to determine the current at other frequencies. The current within each facet is calculated by weighting the current at the edges with their basis functions. Finally, the total scattered field versus frequency is calculated by integrating the extrapolated current. Note that the maximum unambiguous time delay that can be resolved by ESPRIT is inversely proportional to the frequency sampling of the data points. Therefore, to avoid aliasing in the time-of-arrival estimates, the frequency sampling interval must be less than $c/2R_{\max}$ where $R_{\max}$ is the maximum range window of the target. Typically, we choose $R_{\max}$ to be about twice the target size to accommodate most of the times-of-arrival associated with the multiple scattering mechanisms.

III. Range Profile Generation

We first consider a 2-D cylinder-plate target to demonstrate the performance of algorithm. As plotted in the inset of Fig. 2, the diameter of the cylinder is 4.2 m and the length of the plate is 20 m. The distance between the center of the cylinder and the plate is 6.2 m. The incident angle is 45° with respect to the plate. In this structure, the multiple scattering mechanisms between the cylinder and the plate dominate the backscattering. The exact RCS data are calculated for 67 points from 0.3 GHz to 0.63 GHz by a 2-D MoM code. The results are plotted as the dashed curve in Fig. 2. The frequency extrapolation is carried out from the low end of the frequency band to the high end. For this particular example, the model parameters are estimated by ESPRIT from 16 computed points between 0.3 GHz and 0.375 GHz and the model order is chosen to be 4 GHz. From the model, the frequency response is extended up to 0.63 GHz, and plotted as the solid line in Fig. 2. Comparing these two curves, we see that the positions of all the peaks and nulls agree well while the amplitudes show some deviations.

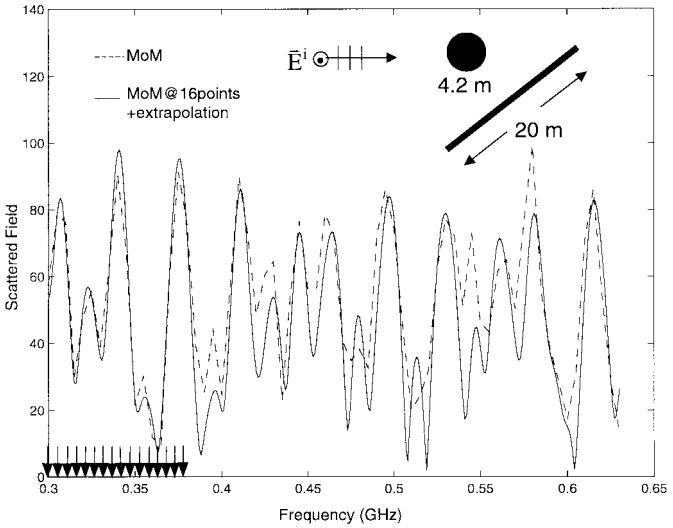

Fig. 2. Comparison of the backscattered field vesus frequency for the (circular cylinder)-(plate) model between the brute-force MoM results and the extrapolated results based on 16 points between 0.3–0.375 GHz.

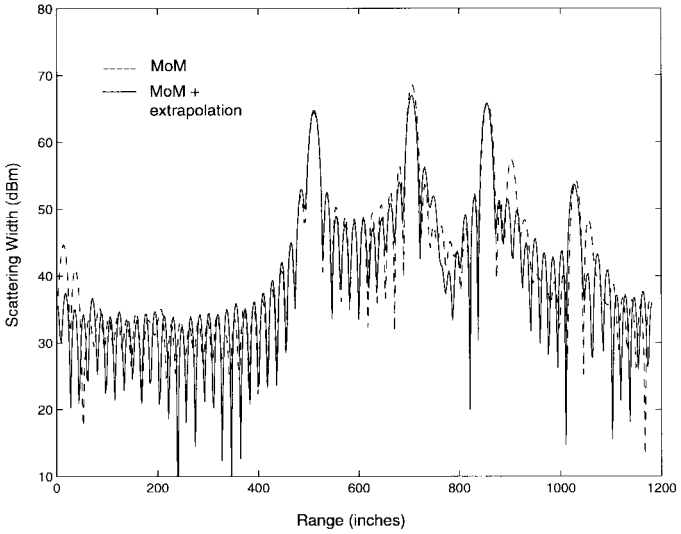

Fig. 3. Comparison between the range profiles obtained by Fourier transforming the frequency responses in Fig. 2.

The average deviation of the extrapolated frequency response from the calculated response is 2.06 dBm. A more detailed error analysis will be conducted in the next section. Note that a point at the high-frequency end requires approximately eight times the computation time of a point at the low-frequency end when using a direct matrix solver. The good agreement in the beatings of frequency responses indicates a good estimate of the time-of-arrivals, i.e., the positions of the scattering features in time. To verify this point, the range profiles are obtained and plotted in Fig. 3 by Fourier transforming the frequency responses. It is found that the main scattering features are very consistent between the two results. The correlation coefficient between the extrapolated range profile and the calculated range profile is 0.98. It is also observed that the extrapolation algorithm fail to predict some of the weaker late-time responses (some of which wrap around to the early time). We believe these late-time responses correspond to the multiple scattering mechanisms whose interaction orders are too high to be modeled by 16 sampling points.

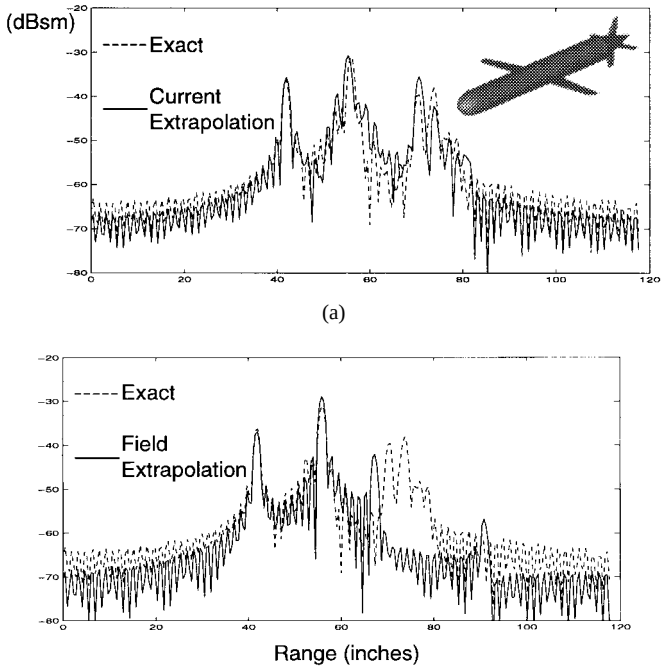

Fig. 4. Comparison between range profiles generated from extrapolation in current and in field. (a) Extrapolation in current (solid line) versus exact (dashed line). (b) Extrapolation in field (solid line) versus exact (dashed line).

In the second example, we consider a 3-D missile model. The target geometry is shown in the inset of Fig. 4(a). The target is approximately 1.3 m in total length. The incident angle is at 30° in azimuth and 0° in elevation. The calculation is done using the MLFMM-based code fast Illinois Sower code (FISC) [12] on an SGI O2 workstation (R10K/155 MHz). A total of 81 frequency points for the horizontal (HH)-polarization are generated between 2–6 GHz using the brute-force approach to produce the reference data. To test the extrapolation algorithm, ten frequency points between 2.50–2.95 GHz are used to extrapolate the induced current over the 2–6 GHz frequency band using a model with $N = 4$. Shown in Fig. 4(a) is the comparison of the range profiles generated using the extrapolated frequency data and the reference frequency data from 2 to 6 GHz. The three main scattering features due to the nose, left wing, and tail fins of the target are well predicted by the extrapolation algorithm. The total computation time for generating the ten frequency points and running the extrapolation algorithm is about 3 h, while the brute-force frequency calculation takes about 80 h on the same machine. As discussed earlier in Section II, the same time-of-arrival model can also be applied directly to the total scattered field instead of the induced current. Shown in Fig. 4(b) is the resulting extrapolated range profile by fitting the scattered field computed at the same ten frequency points to a four-term model. As we can see, while the extrapolation results from current in Fig. 4(a) agree well with the reference results in Fig. 4(b), the extrapolation results from field agree very poorly with the reference results. The last two peaks are totally

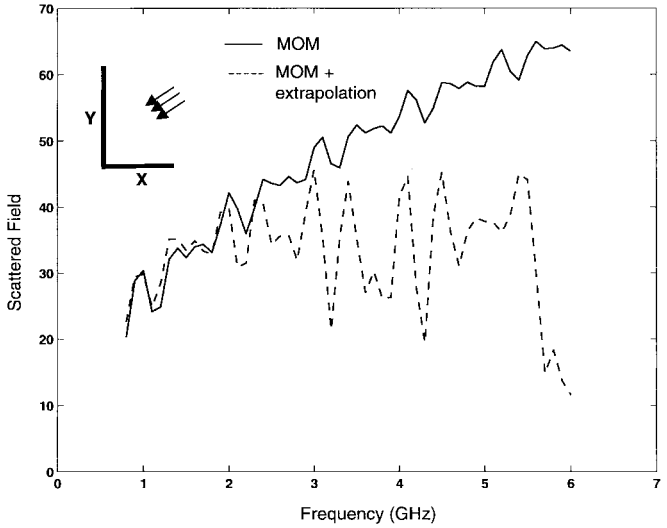

Fig. 5. Comparison of the backscattered field vesus frequency between the brute-force MoM results and the extrapolation results for the dihedral.

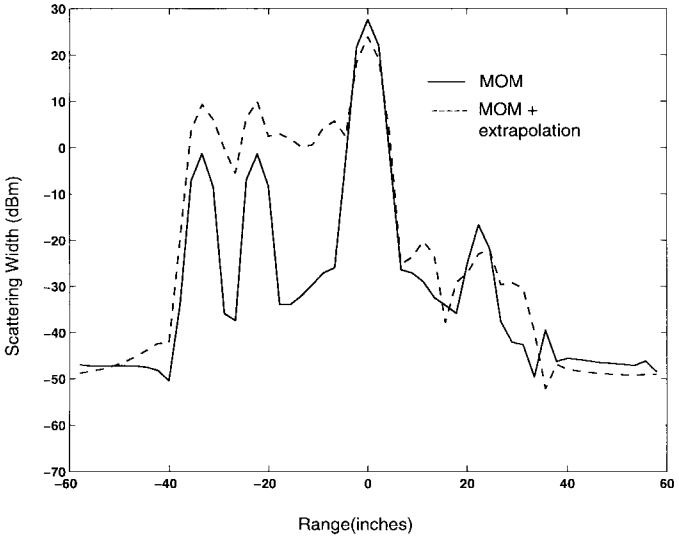

Fig. 6. Comparison between the range profiles of the dihedralobtained by brute-force MoM and MoM + extrapolation.

mispredicted in amplitude and position. This is because the scattered field cannot be modeled adequately by only four terms. However, to increase the model order requires that a larger number of frequency points be computed from the FISC simulation. Therefore, the current parameterization is the superior approach.

IV. Extrapolation Bandwidth

We will now address the issue of extrapolation error. In particular, we set out to find the main factors which influence the accuracy of the extrapolation results and determine an upper limit on the frequency extrapolation bandwidth. A series of numerical experiments are conducted on a 2-D dihedral scatterer. As shown in the inset of Fig. 5, the dihedral is 40 cm long in the x direction and 60 cm long in the y direction, with the vertex at the origin. The incident wave is from 45°. The reference backscattered field versus frequency curve is generated by a 2-D MoM code from 0.8 GHz to 6 GHz at a sampling of 0.1 GHz and is shown as the solid line in Fig. 5. The extrapolation result is shown as the dashed line in the same figure. It is obtained by calculating the current on the dihedral at 8 evenly sampled frequencies between 0.8–1.5 GHz and then extrapolating the current to the whole frequency band. The MoM discretization criterion used to generate the eight samples is ten bases per wavelength at 0.8 GHz. The model order used in the ESPRIT algorithm is chosen as three, with the dihedral scattering mechanism taken into account. We shall introduce two bandwidth terms in assessing the performance of the extrapolation algorithm. The absolute extrapolation bandwidth (AEB) is defined as the ratio between the highest extrapolated frequency and the frequency at which the MoM code is run. To achieve the maximum computation gain, we should always run the MoM code at the low end of the frequency band. Hence, the AEB is approximately the ratio between the highest extrapolated frequency and the lowest frequency in the band. The relative extrapolation bandwidth (REB) is defined as the ratio between the number of points extrapolated and the number of points computed. In the above example $\mathrm{AEB} = (6\ \mathrm{GHz}/0.8\ \mathrm{GHz}) = 7.5$, and $\mathrm{REB} = (53/8) = 6.3$.

The corresponding range profiles from both the reference data and the extrapolated response are plotted in Fig. 6. The strongest peak in the profile is due to the double-bounce retroreflections from the two faces of the corner reflector. The first two range peaks are due to diffractions from the two outer edges. From Figs. 5 and 6, we observe that the extrapolated results are not as good as expected. In Fig. 5, the extrapolated response deviates far away from the reference MoM results beyond 3 GHz, which results in poor target feature prediction in the range profile. The cause can be attributed to spatial aliasing. Since the scattered far field can be considered as the Fourier transform of the induced current, the current must be sampled spatially above the Nyquist rate of two samples per wavelength to avoid aliasing in the calculated scattered field. With the standard discretization of ten bases per wavelength in MoM codes, aliasing is not a concern. However, in our extrapolation, the target is discretized at ten bases per wavelength at the low frequency end. When the current is extrapolated to high frequencies beyond four to five times of the original calculation frequency, the sampling will no longer satisfy the Nyquist criterion. Therefore, the extrapolated scattered field is aliased above 3 GHz in this example. Without increasing the computational burden of the MoM, one possible way to overcome this limit is to interpolate the calculated current to a denser grid using the original basis functions before the extrapolation. In this way the spatial variation of the current phase is better represented for most of the MoM codes where linear or higher order basis functions are used. Once interpolated, the current can be extrapolated in frequency in the denser grid. The scattered field can thus be calculated without serious aliasing. The dashed line in Fig. 7 represents the extrapolated range profile with spatial interpolation of the current at six times the original sampling. Significant improvement is observed when compared to the results in Fig. 6.

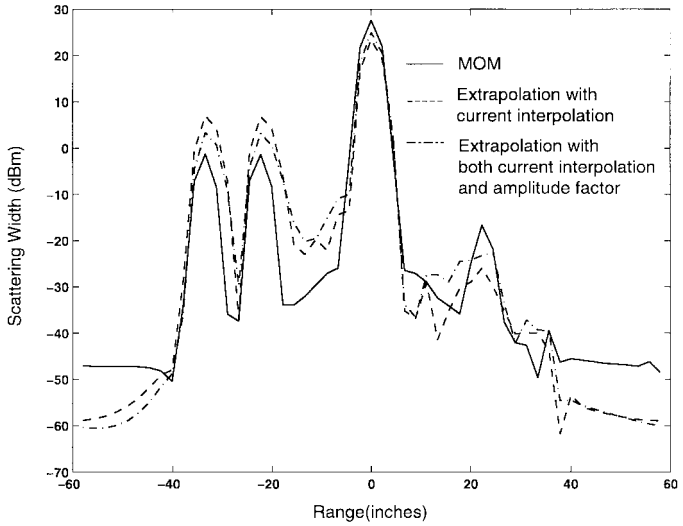

Fig. 7. Comparison between the range profiles of the dihedral obtained by brute-force MoM and MoM with the improved extrapolation techniques.

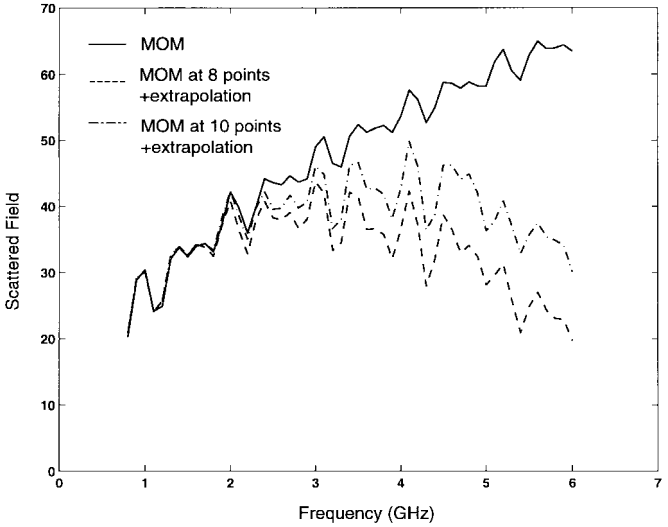

Fig. 8. Comparison of the backscattered field vesus frequency between the brute-force MoM results and the extrapolation resultsusing MOM based on different number of points.

A second source of error is the model error. Note that in (1), the amplitude factors A_i are assumed to be frequency independent, which may not adequately represent real scattering phenomena. For example, it is well known that diffraction currents due to infinite edges have an amplitude frequency dependence of f^{-1}. This could be the reason why the amplitudes of the first two peaks in Fig. 7 are overpredicted by the extrapolation model, as the data are computed in the low-frequency region where the edge diffraction contribution is large and extrapolated based on the frequency-independent amplitude model. As a way to overcome this error, we first run ESPRIT to obtain the time-of-arrival parameters in (1) with frequency independent amplitudes. We then assume each amplitude factor is described by $A_{i0} + A_{i1}f^{-1}$ and use a minimum least-square fit to find these modified amplitude terms. The result is plotted as the dash-dotted line in Fig. 7. We can see it is slightly closer to the original MoM results than the extrapolation results without any frequency dependent terms. More frequency dependent terms can be added to further improve the accuracy. However, this would require more computed data points.

Both the sampling error and the model error discussed thus far limit the AEB of the extrapolation. There is a third error source which impacts the REB. Shown in dashed line in Fig. 8 is the extrapolated frequency response after spatial interpolation and amplitude correction discussed above. We observe that the extrapolation algorithm still has trouble reproducing the upward slope in the reference curve due to the two-bounce retroreflection mechanism as frequency increases. This is reflected in Fig. 7 where the main peak in the range profile from the extrapolation is defocused. We attribute this error to the time-of-arrival estimates from the ESPRIT algorithm. The retro-reflection mechanism arises when the induced current on the dihedral adds coherently in phase to produce a peak in the range profile. However, in the present current-based extrapolation scheme, the phase for each current cell is predicted independently by ESPRIT. Any errors in the time-of-arrival estimate will act as noise and defocus the large

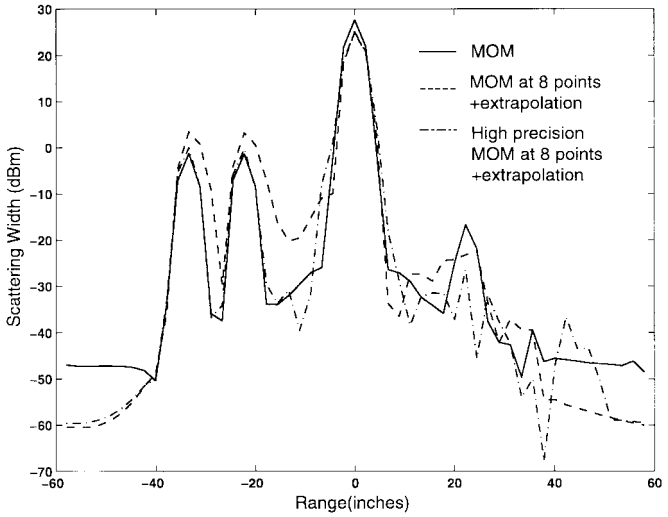

Fig. 9. Comparison of the range profiles between the brute-force MoM results and the extrapolation results using MoM at different precision.

retroreflection. To verify this point, we have closely examined the time-of-arrival estimates in the current and have found that they differ slightly at different points on the dihedral. As discussed in Section II, the accuracy of the ESPRIT algorithm in estimating the correct time-of-arrival is influenced by the finite length of the available data and the noise due to the computation procedure or imperfect modeling. There are two ways to overcome this noise. One is by computing more points. As illustrated by the dash–dotted curve in Fig. 8, we can extend the extrapolation range to a higher frequency by using ten instead of eight computed points. Another way to increase the extrapolation limit is to reduce the numerical noise in the data. As shown by the dash–dotted line in Fig. 9, improvement in the extrapolated range profile is obtained by increasing the MoM discretization to 20 bases per wavelength. In general, an accurate MoM code facilitates an accurate extrapolation.

To summarize, we have determined three error sources, which set limits for the absolute and relative bandwidth of the frequency extrapolation. From our experience with the existing MoM codes and the ESPRIT algorithm, a typical limit is about 4 : 1 for both the AEB and the REB without any of the additional measures like spatial interpolation discussed in this section. In the missile example of [6], an AEB of 1.8 : 1 and an REB of 4 : 1 are achieved if we consider 4.5 GHz to be the upper limit of the extrapolation. Clearly, the REB limit has been reached in this case and we must either compute more points or compute the existing points more accurately to reach a higher absolute extrapolation frequency. Finally, we should point out that the exponential model is based on high-frequency ray-optical behavior of fields and currents. If the computed frequency is not high enough or if high-Q resonance phenomena exist on the target, the performance of the extrapolation will degrade as the order of the model needed to adequately describe such behavior becomes very high.

V. ISAR Image Generation

We next attempt to extend the frequency extrapolation algorithm for range-profile prediction to ISAR image generation. Since ISAR image is a 2-D display of the target scattering features, the scattered field data over multiple look angles and multiple frequencies are required to achieve both cross-range and range resolution. For the new generation of fast MoM codes based on iterative solvers, the calculation has to be repeated for each look angle as well as frequency. To avoid such an exhaustive computation, we combine the frequency extrapolation approach with the well-known bistatic approximation [12], [13] in the angular dimension to generate the required data. In [13], the bistatic field is generated from an MoM code for ISAR imaging. However, no frequency variation of the induced current is considered in the formulation. In our approach, we set out to generate an image which can reproduce the features in a real monostatic ISAR image.

The basic principle of bistatic imaging will be illustrated here in a simplified 2-D form. A general, 3-D derivation can be found in [13]. Based on the physical optics approximation, the scattered field can be written as

$$\begin{aligned} E(K_x, K_y) &= \iint J \cdot e^{-jk_x^s x} e^{-jk_y^s y}\, dx\, dy \\ &= \iint \mathit{Image}(x,y) \cdot e^{-j(k_x^i + k_x^s)x} e^{-j(k_y^i + k_y^s)y}\, dx dy \end{aligned} \tag{4}$$

where J is the induced current and $\mathit{Image}(x, y)$ is the ISAR image of the target. Given the scattered field on a rectangular K_x and K_y grid, the image can be constructed via a 2-D FFT. Depending on whether the scattered field data are collected under the monostatic or the bistatic scenario, the relationships between $K_x - K_y$ and frequency-angle are described as

$$\begin{cases} K_x = 2k_x^s = 2k\cos(\theta_s) \\ K_y = 2k_y^s = 2k\sin(\theta_s) \end{cases} \quad \text{(Monostatic)} \tag{5}$$

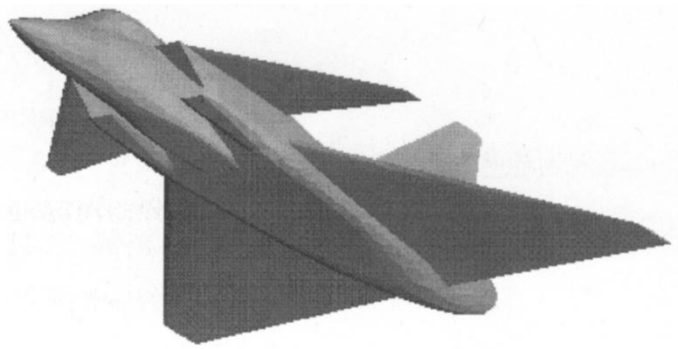

Fig. 10. Geometry of the VFY-218 airplane.

$$\begin{cases} K_x = k_x^i + k_x^s = k[\cos(\theta_i) + \cos(\theta_s)] \\ K_y = k_y^i + k_y^s = k[\sin(\theta_i) + \sin(\theta_s)] \end{cases} \quad \text{(Bistatic)} \tag{6}$$

where k is the free-space wave number, θ_i is the incident angle, and θ_s is the observation angle. In MoM codes based on iterative solvers, it is much less costly to produce the fields in bistatic form than in monostatic form. Once the induced current at one incident angle is computed, the scattered field at multiple observation angles can be generated easily by integrating the current. In our image formation scheme, the current is first calculated at a few low-frequency points and then extrapolated to a broad frequency band. After the current at multiple frequencies are obtained, we integrate the current to find the bistatic scattered fields at different observation angles. If the fields are calculated on a uniform grid in the frequency-angle domain, it will not be on a rectangular grid in the $K_x - K_y$ space after the mapping in (6). Therefore, a reformatting operation is needed before the 2-D FFT algorithm can be utilized for image formation. Alternatively, it is also possible to directly compute the fields on a rectangular grid in the $K_x - K_y$ space.

An example is presented here to verify the image extrapolation algorithm. The target is the benchmark VFY-218 airplane shown in Fig. 10. The fuselage length of the airplane is 15.33 m and the maximum width at the wing tips is 8.90 m. The incident angle is 130° from nose-on and the HH-polarization is considered. We first use FISC to calculate the induced current at ten evenly sampled frequency points between 267 and 294 MHz. Next, the current is extrapolated to a total of 89 frequency points evenly spaced between 267 and 533 MHz. For each frequency point, the bistatic scattered field is computed at 91 observation angles evenly spaced between 90° and 170°. After the reformatting operation and 2-D FFT, the ISAR image of the VFY-218 is generated, as shown in Fig. 11. The resolution in both range and cross range is 0.52 m. The total computation time is 22 h on an SGI O2 workstation with 20 h of FISC computation. If we use the brute-force FISC calculation for every frequency and every monostatic angle, the total computation time would be about 46 046 h or 5.3 years. In Fig. 12, an ISAR image is also generated from the monostatic chamber measurement data for comparison. The data come from the chamber measurement of a 1 : 30 scaled model with frequency bandwidth from 8 to 16 GHz and angle range from 110° to 150° [11]. The target outline is overlaid on the image. Since the model used for the measurement has

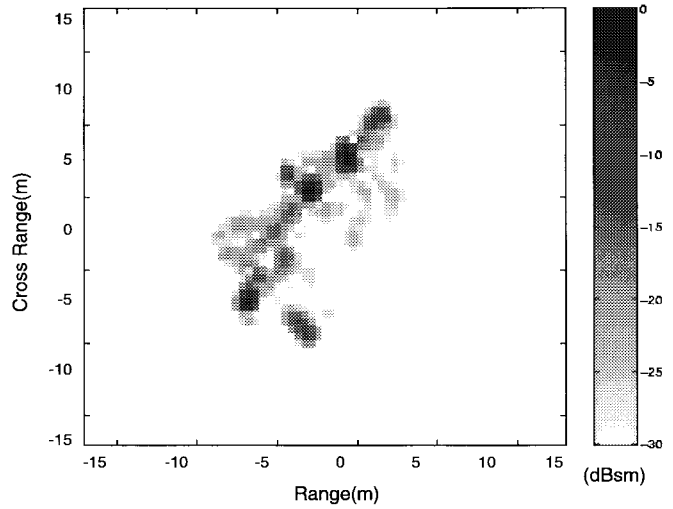

Fig. 11. ISAR image of the VFY-218 constructed from FISC results with frequncy extrapolation and the bistatic approximation.

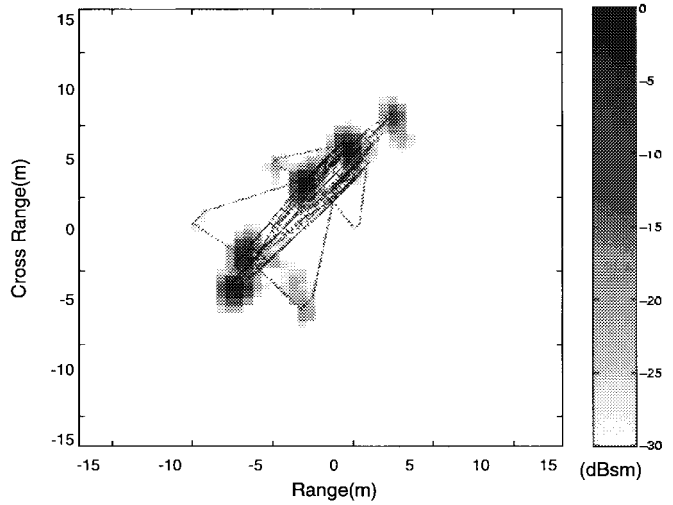

Fig. 12. ISAR image of the VFY-218 constructed from chamber measurement data.

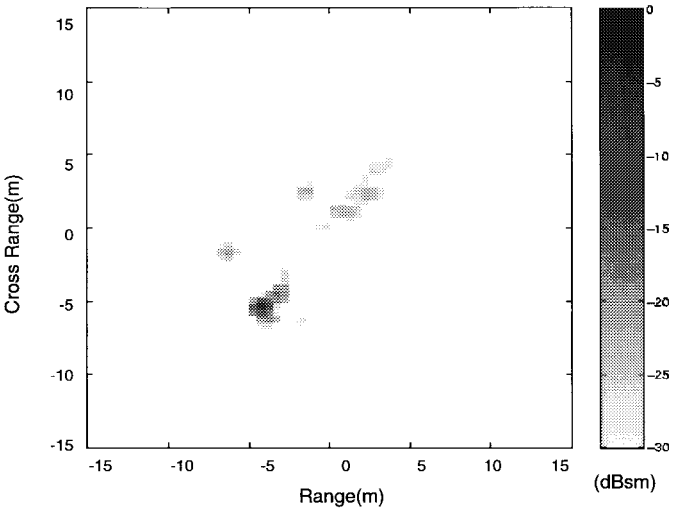

Fig. 13. ISAR image of the VFY-218 constructed from physical optics prediction.

an open exhaust duct, while the CAD model used in the FISC calculation has a sealed duct, it is expected that there are some differences between the two images near the tail region. As we can see, although the predicted image appear to have a smaller dynamic range than the measured one, most of the prominent scattering features in the measured image are well produced in the prediction. The predicted image based on a crude physical optics solution is also generated and shown in Fig. 13. Its agreement with the measured image is very poor.

As a final remark, our present approach for image prediction is based on the bistatic approximation for angular extrapolation. It is well known that the equivalence between bistatic and monostatic data is only valid under the physical optics approximation. As a result, multiple scattering phenomena will not be properly predicted in the extrapolated image. An angular extrapolation approach that can better predict the multiple scattering mechanisms is currently under study [15].

VI. Conclusion

An efficient frequency extrapolation approach has been presented for moment method codes to predict radar signatures. Our approach is to parameterize the current on the target based on a multipath excitation model. Using the ESPRIT superresolution algorithm, we extract the time-of-arrival and amplitude parameters in the model from a limited number of MoM calculations in frequency. The range profiles for a missile model have been calculated in this manner to verify the feasibility and efficiency of the algorithm. Since the algorithm implements the same edge-based basis function as in most of the 3-D MoM codes, it is flexible in dealing with targets with complicated geometry and can be easily used as a general postprocessing tool for MoM codes. The error sources and the limitation of the extrapolation algorithm have been investigated. The concept of absolute and relative extrapolation bandwidth has been proposed to assess the algorithm and determine practical engineering guidelines. Furthermore, the algorithm has been extended to generate ISAR images by using the frequency extrapolation scheme in conjunction with the bistatic approximation for the angular dimension. Good agreement on the dominant scattering features is observed between the predicted image and the measured image of the VFY-218 airplane at 400 MHz.

Acknowledgment

The authors would like to thank Prof. W. Chew and Dr. J. Song for their help in using FISC.

References

[1] R. Coifman, V. Rokhlin, and S. Wandzura, "The fast multiplole method for the wave equation: A pedestrian prescription," *IEEE Trans. Antennas Propagat. Mag.*, vol. 35, pp. 7–12, June 1993.

[2] J. Song, C. C. Lu, and W. C. Chew, "Multilevel fast multipole algorithm for electromagnetic scattering by large complex objects," *IEEE Trans. Antennas Propagat.*, vol. 45, pp. 1488–1493, Oct. 1997.

[3] G. J. Burke, E. K. Miller, S. Chakrabarti, and K. Demarest, "Using model-based parameter estimation to increase the efficiency of computing electromagnetic transfer functions," *IEEE Trans. Magn.*, vol. 25, pp. 2807–2809, July 1989.

[4] K. Kottapalli, T. K. Sarkar, Y. Hua, E. K. Miller, and G. L. Burke, "Accurate computation of wide-band response of electromagnetic systems

utilizing narrow-band information," *IEEE Trans. Microwave Theory Tech.*, vol. 39, pp. 682–687, Apr. 1991.
[5] Z. Altman and R. Mittra, "Combining an extrapolation technique with the method of moments for solving large scattering problems involving bodies of revolution," *IEEE Trans. Antennas Propagat.*, vol. 44, pp. 548–553, Apr. 1996.
[6] Y. Wang, H. Ling, J. Song, and W. C. Chew, "A frequency extrapolation algorithm for FISC," *IEEE Trans. Antennas Propagat.*, vol. 45, pp. 1891–1893, Dec. 1997.
[7] C. J. Reddy, M. D. Deshpande, C. R. Cockrell, and F. B. Beck, "Fast RCS computation over a frequency band using method of moments in conjunction with asymptotic waveform evaluation technique," *IEEE Trans. Antennas Propagat.*, vol. 46, pp. 1229–1233, Aug. 1998.
[8] R. Roy, A. Paulraj, and T. Kailath, "ESPRIT—A subspace rotation approach to estimation of parameters of cisoids in noise," *IEEE Trans. Acoust., Speech, Signal Processing*, vol. ASSP-34, pp. 1340–1342, Oct. 1986.
[9] J. Li and R. T. Compton Jr., "Angle and polarization estimation using ESPRIT with a polarization sensitive array," *IEEE Trans. Antennas Propagat.*, vol. 39, pp. 1376–1383, Sept. 1991.
[10] R. Bhalla, J. Moore, and H. Ling, "A global scattering center representation of complex targets using the shooting and bouncing ray technique," *IEEE Trans. Antennas Propagat.*, vol. 45, pp. 1850–1856, Dec. 1997.
[11] H. T. G. Wang, M. L. Sanders, and A. Woo, "Radar cross section measurement data of the VFY 218 configuration," Tech. Rep. NAWCWPNS TM-7621, Naval Air Warfare Ctr., China Lake, CA, Jan. 1994.
[12] User's Manual for FISC (Fast Illinois Solver Code), Center for Computational Electromagnetics, University of Illinois at Urbana-Champaign and DEMACO, Inc., Champaign, IL, Jan. 1997.
[13] R. Bhalla and H. Ling, "ISAR image formation using bistatic data computed from the shooting and bouncing ray technique," *J. Electromagn. Waves Applicat.*, vol. 7, pp. 1271–1287, Sept. 1993.
[14] J. F. Shaffer, B. A. Cooper, K. W. Hom, R. C. Baucke, and N. A. Talcott Jr., "A review of bistatic k-space imaging for electromagnetic prediction codes for scattering and antennas," *IEEE Antennas Propagat. Mag.*, vol. 39, pp. 21–29, Oct. 1997.
[15] Y. Wang and H. Ling, "A model-based angular extrapolation approach for MoM," submitted for publication in *Microwave Opt. Tech. Lett.*, July 1998.

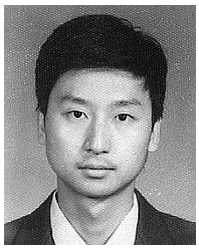

Yuanxun Wang (S'96) was born in 1973. He received the B.S. degree from University of Science and Technology of China, Hefei, in 1993, and the M.S. degree from University of Texas at Austin in 1996, both in electrical engineering. He is working toward the Ph.D. degree from University of Texas at Austin.

Since 1995, he has worked as a Research Assistant in the Department of Electrical and Computer Engineering, University of Texas at Austin. His research interests include modeling and simulation of electromagnetic scattering, multispectral and adaptive signal processing, SAR/ISAR image processing, microwave, and millimeter-wave system development.

Hao Ling (S'83–M'86–SM'92–F'99), for a photograph and biography, see p. 227 of the February 1997 issue of this TRANSACTIONS.